The structural basis for the self-inhibition of DNA binding by apo-σ^{70}

Khalil Joron[1], Joanna Zamel[1], Shani Dvir[1], Nir Kalisman[1,2], Eitan Lerner[1,2]*

Affiliations

[1] Department of Biological Chemistry, Alexander Silberman Institute of Life Sciences, Faculty of Mathematics & Science, Edmond J. Safra Campus, Hebrew University of Jerusalem; Jerusalem 9190401, Israel.

[2] Center for Nanoscience and Nanotechnology, Hebrew University of Jerusalem; Jerusalem 9190401, Israel.

* Corresponding author. Email: eitan.lerner@mail.huji.ac.il

Abstract

Initiation of transcription in *Escherichia coli* is facilitated by promoter specificity factors, such as σ^{70}, which bind promoter dsDNA when in complex with RNA polymerase (RNAP), in which it is in an extended conformation with solvent-exposed DNA-interacting residues. If so, what in the structure of apo-σ^{70} prevents binding to promoter dsDNA at high affinity? By performing cross-linking mass spectrometry (CL-MS) and integrative structural modelling we elucidate structure models of apo-σ^{70} that exhibit burial of almost all DNA-binding residues. *In vivo* CL-MS detects crosslinks unique to the compact fold of apo-σ^{70} that occur at stationary growth phase. Conclusively, we provide structural information to show that the high affinity DNA-binding capabilities of apo-σ^{70} are conformationally-inhibited and can be activated mostly in the context of transcription.

One-Sentence Summary: This work provides a structural mechanism for why apo-σ^{70} does not bind promoters at high affinity when it is not in the direct context of transcription.

Main Text

σ promoter specificity factors are well-known as proteins that facilitate specific binding of RNA polymerase (RNAP) to gene promoters in bacteria(*1*, *2*). Among the different types of σ factors in *E. coli*, σ^{70} binds promoters of house-keeping genes, mostly under normal growth conditions at log phase(*3*). The mechanism of initiating DNA transcription involves the binding of σ^{70} onto the DNA promoter sequence, only when σ^{70} is part of the RNAP holoenzyme complex(*4*). To form the RNAP-σ^{70} complex, better known as the RNAP holoenzyme, σ^{70} adapts the structural organization, in which σ^{70} regions 2 and 4 (σR2 and σR4, respectively) bind core RNAP β-β' RNAP subunits, with σR4 binding the β subunit on one far end of the complex, and σR2 binding the β' subunit at the other far end. Then, in the context of the RNAP holoenzyme, proper binding of the σ^{70} subunit to a promoter initially forms the RNAP-promoter closed (RP_C) complex, where σR4.2 binds the -35 promoter element, σR2.3 and σR2.4 bind the -10 promoter element, σR1.2 binds the promoter discriminator sequence, σR3 interacts with the -10 upstream extended element and the C-terminal domain of the α subunit dimer of RNAP also interact with the promoter UP element(*5*). The formation of the RP_C is then followed by a cascade of DNA isomerization events(*6–10*), which end with a stretch of 10-12 bases of promoter DNA right upstream to the transcription start site that melts and forms the DNA transcription bubble, stabilized within the RNAP-promoter open (RP_O) complex(*11*, *12*). Importantly, throughout transcription initiation complex, σ^{70} exhibits an extended structure, whereby σR2 and σR4 are far apart from each other, to facilitate proper promoter binding. However, as all proteins including σ^{70} are synthesized separately, σ^{70} may exist in bacteria also in an unbound form, at least until it binds to RNAP. When σ^{70} is not bound to RNAP, it can bind anti-σ factors that will repress transcription by competing with RNAP on the interaction with σ^{70} and even by sequestering σ^{70} out of the cytoplasm(*13–15*). Yet, different factors may lead to the release of σ^{70} from its interaction with anti-σ factors, and back into the cytoplasm, until it rebinds RNAP(*16–19*). Therefore, this process among others might dictate the lifetime in which σ^{70} will exist in an unbound form.

Structurally, the protein databank (PDB) includes many entries of the transcription initiation complex, including with σ^{70} as a subunit within these complexes(*4*, *8*, *20–30*). Exploring the PDB for σ^{70} structures not in the context of RNAP identifies only a few *E. coli* structures of separate σ^{70} regions, such as σR4 bound to several transcription factors(*31–33*), the unbound σR2(*34*, *35*), as well as the structures of regions of house-keeping σ factors from other bacteria(*35*, *36*). Yet, to the best of our knowledge, a structural description of the full-length apo-σ^{70} has not yet been reported. Still, there have been *in vitro* biochemical reports showing that apo-σ^{70} adopts a predominant distinct compact conformation(*37–40*), which undergoes an overall structural reorganization upon binding core RNAP, inducing a transition from an unbound state to the RNAP-bound state(*41–45*). In that respect, it is noteworthy that the σ^{70} regions are connected by flexible peptide linkers(*35*), and upon binding to RNAP to form the holoenzyme, the σ^{70} regions preserve their fold, while the linkers extend and allow the reorganization of the σ^{70} regions one relative to the other(*46–48*).

If so, what are the structures and conformations of σ^{70} as an unbound protein, apo-σ^{70}, in solution? To answer this question, we first perform single-molecule Förster resonance energy transfer (smFRET)(*49*, *50*) experiments to show that apo-σ^{70} is found predominantly in a compact conformation, and that free promoter dsDNA in the absence of RNAP can induce a low amount of small conformational changes in apo-σ^{70} only at low affinity. Relying on the fact that most of apo-σ^{70} in solution is found in one predominant conformation, we perform *in vitro* cross-linking mass-

spectrometry (CL-MS) experiments(*51–57*) on purified recombinant σ^{70}. Then, we compare the resolved pairs of residues and their recovered C_α-C_α distance ranges to the same features in existing PDB structures of full-length σ^{70}. Our results can be explained only if the apo-σ^{70} has a more compact structure than those provided in the PDB. To provide a working structure model of the apo-σ^{70}, we used the CL-MS inter-residue spatial information as restraints to drive PatchDock(*58, 59*) integrative structural modeling of σ^{70}. The resulting structure models of apo-σ^{70} confirm the compact structural organization between σ^{70} regions and provide insights as to why apo-σ^{70} is unable to bind dsDNA at high affinity when it is not part of the transcription complex.

Finally, results from *in vivo* CL-MS on σ^{70} in *E. coli* report on abundance of inter-residue proximities unique to the compact apo-σ^{70} conformation, not in log phase when σ^{70} is recruited for transcription, but rather in the stationary bacterial growth phase when alternative σ factors are recruited for transcription.

Single-molecule Förster resonance energy transfer of dual labeled σ^{70}

A FRET donor dye (ATTO 550) and acceptor dye (ATTO 643) were conjugated through stochastic labeling to cysteines at residues 442 and 579 of σR2 and σR4, respectively (see *Supplementary Materials*). The conformation of apo-σ^{70} was first examined with smFRET (Fig. 1, A), and exhibited results consistent with previously published data of similar smFRET measurements(*40*): a predominant FRET sub-population with high FRET efficiency that can be explained by a conformation of the apo-σ^{70} with regions 2 and 4 in close proximity. Importantly, the dyes labeling these residues of the RNAP-bound extended conformation of σ^{70}, is expected to yield a FRET efficiency of ~0.5(*40*). Further analysis using multi-parameter photon-by-photon hidden Markov modeling (mpH^{2}MM)(*60*) shows transitions in the tens of ms (table S1) between a major FRET sub-population with high mean FRET values (fig. S1, A, blue and red) and a minor FRET sub-population with slightly lower FRET efficiency (fig. S1, A, green), which represent a predominant compact and a minor populated less compact σ^{70} conformation, but surely not the fully extended one (i.e., it is expected to exhibit a mean FRET efficiency of ~0.5). Yet most of the protein in apo form exhibits a high FRET sub-population that is associated with a compact conformation (Fig. 1, A and fig. S1, A). Incubating the dye-labeled σ^{70} with 2 µM dsDNA lacCONS promoter(*61, 62*) leads to a small fraction of σ^{70} molecules to exhibit a FRET sub-population at slightly lower FRET efficiency, which corresponds to a larger distance between σR2 and σR4 (Fig. 1, C and fig. S1, C). However, at 100 nM of the promoter dsDNA this conformational change still exists (fig. S1, B, green), but its population decreases to that in the absence of dsDNA (Fig. 1, B), which can only be seen after mpH^{2}MM analysis. The transition rates from the compact conformation represented by the high FRET sub-populations to a less compact one represented by a slightly lower FRET sub-population, are of tens of ms, increasing to hundreds of ms in the presence of dsDNA. In previous smFRET studies of σ^{70} it was shown that in the presence of RNAP, 500 nM promoter dsDNA was sufficient to induce a full FRET shift towards mid-FRET values(*40*). In fact, other smFRET studies also show that in the presence of RNAP a full shift of FRET values occurs at only few nM of dsDNA (*9, 10*). Therefore, apo-σ^{70} can bind dsDNA in a nonspecific manner only at low affinity (fig. S1), and binding of σ^{70} to RNAP activates its high affinity binding capabilities to dsDNA promoters.

In summary, the smFRET results suggest that apo-σ^{70} is in an equilibrium between two states, a predominant compact conformation and a minor slightly less compact conformation that is still more compact than the fully extended one. Therefore, we can assume that C_α-C_α distances between σ^{70} regions that are far apart in the RNAP-bound extended conformation, which should not yield

close proximities, would yield the short proximities that will allow crosslinking to occur efficiently in the apo form. Therefore, we set to explore the structural features of the predominant compact apo-σ^{70} conformation using CL-MS and integrative structural modeling.

Unique features of apo-σ^{70} relative to existing structures

We performed *in vitro* CL-MS after validating that σ^{70} is transcriptionally active (fig. S2). Then, we attained short- and intermediate-scale spatial information, by using the zero-length primary amine to carboxylate coupler 4-(4,6-dimethoxy-1,3,5-triazin-2-yl)-4-methyl-morpholinium chloride (DMTMM)(*53*) and the primary amine to primary amine crosslinker bis(sulfosuccinimidyl)-substrate (BS^3), which report on pairs of residues within C_α-C_α distances <16 or <30 Å, respectively(*53*) (see *Supplementary Materials*). The high-ranking crosslinking results are summarized in tables S2 and S3 for BS^3 and DMTMM, respectively. The interconnectivity between σ^{70} regions is graphically shown in an arcs diagrams (fig. S3), including ones expected to be distanced from each other (e.g., σR2 and σR4) as seen in PDB structures of the RNAP-bound σ^{70} (see tables S2 and S3, in red). We test the satisfaction of the recovered inter-residue distance ranges against the inter-residue distances in existing PDB structures of the RNAP-bound σ^{70} in the context of holoenzyme (Fig. 2), RP_O (fig. S4), and transcription initiation ternary complexes other than RP_O (fig. S5). In all RNAP-bound σ^{70} PDB structures of all transcription initiation states, 43-46% of the BS^3 crosslinking data, and 25-38% of the DMTMM crosslinking data fit within the structural coordinates (Fig. 2, and figs. S4, S5). Performing the same test on a structure model we predicted using RoseTTAFold(*63*), we find the same level of agreement with the crosslinking data (Fig. 3, A). Following that, we find similar results also with model structures produced by AlphaFold2(*64*, *65*) and by OmegaFold(*66*). Across all PDB structures tested, we detect the same crosslinked pairs of residues that do not agree with the spatial distances presented in the PDB structures. Interestingly, these crosslinks include mostly ones connecting σR4 and σR3 with σR2.

Integrative structure models of apo-σ^{70}

Results of smFRET together with the large fraction of residue pairs that were found to be in close proximity, unlike their larger distances in the RNAP-bound σ^{70} structures, warrants the use of the CL-MS data as restraints in modeling the potential structure of the apo-σ^{70}. Importantly, we do not identify any crosslinked pairs of residues involving the σR1.1, probably due to it being connected via a disordered linker(*5*). Also, crosslinks within the same region were not used in the docking process since we treat the regions as rigid building blocks, which do not change their fold. Instead, we use the crosslinks that were not used as restraints for validating the resulting structure models. Structural comparison of σR2 and σR4 of the full length RNAP-bound σ^{70} to the NMR structures of σR2 and σR4 alone, shows that in both cases the domains indeed maintain their overall fold(*31*). Using the CL-MS derived spatial restraints, we perform docking between the regions, using PatchDock(*59*), on pair of consecutive regions at a time (see *Supplementary Materials*). In this iterative approach, we make sure to start with the structural parts that include a large number of crosslinked pairs of residues, and hence their results are more constrained and include less degrees of freedom. The stepwise results of the process, and the final structure models are shown (Fig. 4, A). Inspecting the attained structure models of apo-σ^{70} against the crosslinking data, we achieve a significant increase in the percentage of crosslinks that are now found within the cutoff distances covered by the crosslinkers. The compact structure of the apo-σ^{70} retrieved from PatchDock exhibits an addition of up to 36% BS^3 CL-MS data, and an addition of up to 15% with DMTMM

crosslinking data (Fig. 4, B), relative to the results of the comparisons against the extended conformation of σ^{70} in the RNAP-bound PDB structures.

Structure-function comparisons of apo-σ^{70} structure models against RNAP-bound structures

Next, we perform a comparison between the top-ranking structure models we recovered for the apo-σ^{70} against the RNAP-bound σ^{70} structure predicted using RoseTTAFold, which turns out to yield a similar structure model as other existing prediction algorithms, such as AlphaFold2 as well as OmegaFold (see *Supplementary Materials*). We perform structural comparisons to assess the validity of the resulting structure models, by comparing regions of exposed or buried residues, and residues potentially interacting with RNAP or DNA. Comparison of σR1.2 and σR2 residues of the structure models and the RNAP-bound σ^{70} structure, within the RNAP holoenzyme, reveals exposed residues of σR1.2 in both compact and extended structures, whereas these residues are known to interact with the promoter discriminator sequence and with the β' RNAP subunit within transcription initiation ternary complexes, (Fig. 5, A). In the RNAP-bound σ^{70}, σR2 residues that act as recognition determinants in binding the core RNAP β` and the -10 promoter sequence, are exposed and hence can be available for interaction with proximal residues (Fig. 5, B). However, while some of the residues interacting with the β` RNAP subunit at RNAP-bound stages remain on the outer surface in the PatchDock-based structure models of apo-σ^{70} (e.g., R373, K377, E381, L384, Q400, L402, D403, Q406 and N409), the σ^{70} residues that construct the recognition site for the -10 promoter sequence are mostly buried inside the compact conformation of apo- σ^{70} due to the interaction of σR2 with σR3 and σR4 (Fig. 5, B). This suggests that an initial interaction of exposed σ^{70} residues with residues of RNAP is required for enabling the exposure of all DNA binding residues in σ^{70}, and by that further facilitating its specific DNA binding capabilities.

The organization of σR4 on top of σR3 within the PatchDock-based structure models of the apo-σ^{70}, shield σR4 residues that otherwise directly interact with the -35 promoter element. However, RNAP interacting residues are left exposed on the outer surface of the structure (Fig. 6, A). Taking a closer look at σR3, in the PatchDock-based structure models of apo-σ^{70}, we notice that most residues that at later transcription initiation stages interact with the template strand DNA, and all residues that interact with the nontemplate strand DNA are buried inside the structure and are hence inaccessible. Moreover, most residues that interact with the β and β' RNAP subunits are located on the exterior surface of σR3.2 and extending through the flexible linker connecting σR3 to σR4 (Fig. 6, A). Therefore, these residues are likely to interact first with RNAP, most probably through σR3.2 interaction with the region of RNAP that forms the RNA exit channel. As for σR4 itself, while residues that at later stages interact with the -35 promoter element within the transcription initiation complex are spotted on the surface of the RNAP-bound σ^{70}, these residues are located on the interior of the PatchDock-based structure models of apo-σ^{70} (Fig 6, B). This suggests, there is little to no interaction between the closed form of σR4 in apo-σ^{70} and DNA prior to RNAP holoenzyme formation. Interactions of σR4 with RNAP are through the β-flap and the β' subunit. Although σR4 is organized in close proximity to σR3 in the PatchDock-based structure models, the residues interacting with the β and β' subunits are exposed on the surface of the protein both in the extended and compact structures of σ^{70} (Fig 6, B). Nevertheless, in the compact apo-σ^{70} structure models, the linker connecting σR4 to σR3 (determining the position of the σR4-RNAP interface) is retracted (Fig 6, A). Therefore, the extension of the linker should occur first to enable the subsequent full interaction of σR3 and σR4 with RNAP β and β' subunits, as part of forming the RNAP holoenzyme, which is only possible through initial σR3 interaction with the RNAP. This is indeed consistent with previous knowledge, where it was shown that truncation of the linker

causes release of the σR4(*46*, *48*). All of the above, support the notion of holoenzyme formation prior to DNA interaction, which then enables full σ^{70}-DNA binding in context of transcription.
Furthermore, we use the electrostatic maps of the core RNAP (PDB code: 3LU0(*67*)) and the RNAP-bound σ^{70} (PDB code: 6PSQ(*8*)) structures generated via the APBS Electrostatics software(*68*) using PyMOL, as well as the PDB structure of the RP_C complex (PDB code: 6PSQ), and the tool PDBePISA(*69*) as a means to forming a hypothesis on the initial interaction between σ^{70} and RNAP. Within the transcription complex, σR1.1, σR3 and σR4 may interact with β and β` subunits, and σR1.2 and σR2 may interact only with β` subunit. While the extended structure of σ^{70} exhibits surface-exposed residues that interact with the β and β` subunits of RNAP, some of these residues appear to be buried in the PatchDock-based structure. Accordingly, we propose that specific interactions of the exposed residues are required to enable full interaction between σ^{70} and RNAP to properly form the RNAP holoenzyme. Generated electrostatic maps of the core RNAP and σ^{70} structures show that the β- σ^{70} and β`-σ^{70} binding interfaces are positively charged (fig. S6, A), while the interacting interface of σ^{70} in the apo-σ^{70} structure is negatively charged (e.g., σ^{70} regions 1.1, 1.2, 2.2, 3.2 and 4.1; fig. S6). While these σ^{70} regions are exposed in the extended RNAP-bound σ^{70} structure (fig. S6, A), the electrostatic map of the PatchDock-based structure reveals how all negatively-charged regions that potentially interact with the core RNAP are buried, except for σR3.2 and the linker connecting it to σR4.1 (fig. S6, B). Next, we examined σ^{70} residues within the structure of RP_C that interface with the RNAP β or β' subunits. Within the compact structure of apo-σ^{70}, ~60% of σR3.2 residues that potentially interact with the β or β`subunits of the RNAP are either negatively-charged (e.g., E532, D528, E527, D524, D519, E518 and E511) or polar (e.g., S520, T512, S509) residues (fig. S7). These residues are potential candidates for making initial σ^{70}-RNAP contacts. Interaction of these residues may lead to extensions of the σR3.2-σR4.1 linker, which causes the conformational change bringing σR4 closer to its interaction site with the β-flap and the zinc finger motif on the β` subunit to help lock σR4 in place.
Overall, the compact predominant conformation of apo-σ^{70} buries most of the DNA interacting residues making them inaccessible, while some RNAP interacting residues are exposed, which supports the notion of RNAP holoenzyme formation as a necessary step for activating σ^{70}'s specific promoter binding capabilities.

Finally, after providing structure models of apo-σ^{70} and potential roles in RNAP binding recognition and regulation of the DNA binding domains of σ^{70}, all *in vitro*, we explore the possibility that the recovered apo-σ^{70} conformation, or at least its unique structural characteristics, exist also in living *E. coli* cells.

CL-MS in E. coli identifies apo-σ^{70} occurs in living bacterial cells

Next, we explore if unique signatures of the compact conformation of apo-σ^{70} appear in *E. coli* cells. We performed *in vivo* CL-MS (see *Methods*) during the logarithmic and stationary bacterial growth phases, using disuccinimidyl suberate (DSS) as crosslinker, which shares the same end-to-end length and crosslinking chemistry as BS^3, but unlike BS^3 is capable of passively crossing into cells. During the stationary phase σ^{38} (i.e., σ^S) replaces σ^{70} in binding RNAP, swapping most of the σ^{70}, which should now be in the apo form(*70*). Ultimately, this enrichment of apo-σ^{70} should introduce unique inter-residue close proximities between pairs of residues that can be explained only by the compact conformation of apo- σ^{70} and were previously captured during the *in vitro* experiments using BS^3 as crosslinker. Out of the 49 crosslinked pairs of residues that we attained *in vitro* and could not explain by the extended RNAP-bound σ^{70} structure, we identified 11 of them again *in vivo* not during the log phase, but rather during the stationary phase (table S2). This finding by itself suggests that a conformation of σ^{70} that resembles the compact apo-form exists also in the

cell, in a state in which apo-σ^{70} can be anticipated. The crosslinked pairs of residues captured *in vivo* are displayed on top of the compact structure 1 retrieved from PatchDock, and the extended structure model retrieved from RoseTTAFold (Fig. 3, B). Out of all crosslinked pairs of residues captured *in vivo* during the stationary phase >70% can be explained by the PatchDock compact apo-σ^{70} conformation, compared to 51% agreement with the extended conformation (Fig. 3, B). During the log growth phase, the housekeeping σ factor, σ^{70}, is mostly bound to the RNAP to enable synthesis of proteins necessary for exponential growth. Therefore, all crosslinked pairs of residues captured in log phase agree with the extended structure, while crosslinks that represent the compact structure were not captured at all (fig. S8).

Discussion

In this work, we provide evidence that apo-σ^{70}, unbound to RNAP, is in a compact conformation, in which σR2 is in close proximity to σR3 and σR4, as shown also by previous works(*37–40*). We elucidate a structure model of the apo-σ^{70} and demonstrate that most of its DNA binding residues are deeply buried, and therefore inaccessible. The buried residues may become accessible mostly upon holoenzyme formation, where σ^{70}'s conformational change is induced, making DNA binding more efficient.

In vitro CL-MS is limited in that it reports solely on pairs of residues that were within a given distance range and not on the pairs of residues that were at longer distances (for further discussion of the CL-MS data see Supplementary text). Therefore, it raises the question of whether or not the extended conformation of σ^{70} also exists intrinsically and dynamically in apo-σ^{70}. In fact, smFRET studies by Vishwakarma, Cao *et al.* suggested that such intrinsic conformational dynamics may exist in *E. coli* apo-σ^{70}(*40*). In their work, they show that the FRET efficiencies between a donor dye labeling residue 579 of σR4 and an acceptor dye labeling residue 442 of σR2 are grouped into a predominant high-FRET sub-population, and a minor mid-FRET sub-population. Using the same labeling positions with different dyes we attain similar results. Overall, both results point towards a preexisting conformational equilibrium between a predominant compact conformation and a minor less compact conformation of apo-σ^{70}, and that introducing RNAP and nanomolars of dsDNA promoter is enough to fully extend the conformation of σ^{70}. Similar smFRET measurements done in this work on apo-σ^{70} in the presence of dsDNA demonstrate that high dsDNA concentration in the absence of RNAP may still induce partial DNA binding of σ^{70}, perhaps through the few already exposed DNA-binding residues. However, the majority of σ^{70} stays in the high FRET sub-population. In the presence of lower dsDNA concentrations, changes to the amount of molecules in each FRET sub-population are not observed (for further discussion see Supplementary text). Overall, these results show that σ^{70} may partially bind dsDNA in the absence of RNAP, and at low affinity, as opposed to DNA binding in the presence of RNAP occurs at high affinity. In that respect, it is important to mention that σ^{70} has been reported to bind DNA structures that deviate from the dsDNA one (e.g., ssDNA in aptamers)(*45*), however not necessarily to dsDNA, and even if yes, not necessarily at high affinities. Most importantly, apo-σ^{70} is found predominantly in the compact conformation, which warrants the use of CL-MS to objectively report on spatial features of its underlying structure that was not yet resolved.

A major achievement presented in our work is the integrative structure model of apo-σ^{70}. However, the question that is left, is whether or not this conformation exists also in *E. coli*. *In vivo*, we managed to capture pairs of residue distances, which were captured also *in vitro* and can only be described by the compact conformation of apo-σ^{70}. Importantly, this finding might report on a biologically-relevant event, where σ^{70} exists in the bacterial cell in stationary phase in an unbound state, rather than being degraded, as presented in the models. Nevertheless, we do take into account the fact that these results were achieved using a high copy number plasmid of σ^{70}, and hence might also be influenced by over-expression effects. If over-expression would serve a problem, we would expect to observe the unique crosslinking signatures of the compact apo-σ^{70} conformation also in log-phase. However, none of them appeared in log-phase, which serves to show that over-expression effects probably do not introduce artificially high numbers of leftover unbound σ^{70}.

In summary, we propose integrative structure models of apo-σ^{70} as means to show the general structural organization in the compact conformation, that buries its DNA-binding residues, and by that self-inhibit the high affinity promoter binding capabilities σ^{70} has only upon activation by binding to RNAP and inducing a conformational change that exposes these residues.

References and Notes

1. R. R. Burgess, "Sigma Factors" in, S. Brenner, J. H. B. T.-E. of G. Miller, Eds. (Academic Press, New York, 2001; https://www.sciencedirect.com/science/article/pii/B0122270800011927), pp. 1831–1834.
2. A. Feklístov, B. D. Sharon, S. A. Darst, C. A. Gross, Bacterial Sigma Factors: A Historical, Structural, and Genomic Perspective. *Annual Review of Microbiology*. **68**, 357–376 (2014).
3. M. S. B. Paget, J. D. Helmann, The σ70 family of sigma factors. *Genome Biology*. **4**, 203–203 (2003).
4. K. S. Murakami, X-ray Crystal Structure of Escherichia coli RNA Polymerase σ70 Holoenzyme. *Journal of Biological Chemistry*. **288**, 9126–9134 (2013).
5. M. C. Davis, C. A. Kesthely, E. A. Franklin, S. R. MacLellan, The essential activities of the bacterial sigma factor. *Canadian Journal of Microbiology*. **63**, 89–99 (2016).
6. R. M. Saecker, M. T. Record, P. L. deHaseth, Mechanism of Bacterial Transcription Initiation: RNA Polymerase - Promoter Binding, Isomerization to Initiation-Competent Open Complexes, and Initiation of RNA Synthesis. *Journal of Molecular Biology*. **412**, 754–771 (2011).
7. F. E. Ruff, T. M. Record, I. Artsimovitch, Initial Events in Bacterial Transcription Initiation. *Biomolecules*. **5** (2015), doi:10.3390/biom5021035.
8. J. Chen, C. Chiu, S. Gopalkrishnan, A. Y. Chen, P. D. B. Olinares, R. M. Saecker, J. T. Winkelman, M. F. Maloney, B. T. Chait, W. Ross, R. L. Gourse, E. A. Campbell, S. A. Darst, Stepwise Promoter Melting by Bacterial RNA Polymerase. *Molecular Cell*. **78**, 275-288.e6 (2020).
9. A. Mazumder, R. H. Ebright, A. N. Kapanidis, Transcription initiation at a consensus bacterial promoter proceeds via a 'bind-unwind-load-and-lock' mechanism. *eLife*. **10**, e70090–e70090 (2021).
10. A. M. Malinen, J. Bakermans, E. Aalto-Setälä, M. Blessing, D. L. V. Bauer, O. Parilova, G. A. Belogurov, D. Dulin, A. N. Kapanidis, Real-Time Single-Molecule Studies of RNA Polymerase–Promoter Open Complex Formation Reveal Substantial Heterogeneity Along the Promoter-Opening Pathway. *Journal of Molecular Biology*. **434**, 167383–167383 (2022).
11. B. Bae, A. Feklistov, A. Lass-Napiorkowska, R. Landick, S. A. Darst, Structure of a bacterial RNA polymerase holoenzyme open promoter complex. *eLife*. **4**, e08504–e08504 (2015).
12. J. D. Helmann, Where to begin? Sigma factors and the selectivity of transcription initiation in bacteria. *Molecular Microbiology*. **112**, 335–347 (2019).
13. D. Missiakas, S. Raina, The extracytoplasmic function sigma factors: role and regulation. *Molecular Microbiology*. **28**, 1059–1066 (1998).
14. J. D. Helmann, Anti-sigma factors. *Current Opinion in Microbiology*. **2**, 135–141 (1999).
15. M. S. Paget, Bacterial Sigma Factors and Anti-Sigma Factors: Structure, Function and Distribution. *Biomolecules*. **5** (2015), doi:10.3390/biom5031245.
16. J.-G. Kang, M. S. B. Paget, Y.-J. Seok, M.-Y. Hahn, J.-B. Bae, J.-S. Hahn, C. Kleanthous, M. J. Buttner, J.-H. Roe, RsrA, an anti-sigma factor regulated by redox change. *The EMBO Journal*. **18**, 4292–4298 (1999).
17. J. Pané-Farré, R. J. Lewis, J. Stülke, The RsbRST Stress Module in Bacteria: A Signalling System That May Interact with Different Output Modules. *Microbial Physiology*. **9**, 65–76 (2005).
18. J. Heinrich, T. Wiegert, Regulated intramembrane proteolysis in the control of extracytoplasmic function sigma factors. *Research in Microbiology*. **160**, 696–703 (2009).
19. F.-C. Anne, F. Julia, R. Christian, E. J. Zingg, G. Benjamin, V. J. A., Sigma factor mimicry involved in regulation of general stress response. *Proceedings of the National Academy of Sciences*. **106**, 3467–3472 (2009).
20. U. Mechold, K. Potrykus, H. Murphy, K. S. Murakami, M. Cashel, Differential regulation by ppGpp versus pppGpp in Escherichia coli. *Nucleic Acids Research*. **41**, 6175–6189 (2013).
21. B. Bae, E. Davis, D. Brown, E. A. Campbell, S. Wigneshweraraj, S. A. Darst, *Proceedings of the National Academy of Sciences*, in press, doi:10.1073/pnas.1314576110.
22. D. Degen, Y. Feng, Y. Zhang, K. Y. Ebright, Y. W. Ebright, M. Gigliotti, H. Vahedian-Movahed, S. Mandal, M. Talaue, N. Connell, E. Arnold, W. Fenical, R. H. Ebright, Transcription inhibition by the depsipeptide antibiotic salinamide A. *eLife*. **3**, e02451–e02451 (2014).
23. Y. Zuo, T. A. Steitz, Crystal Structures of the E. coli Transcription Initiation Complexes with a Complete Bubble. *Molecular Cell*. **58**, 534–540 (2015).
24. A. Narayanan, F. S. Vago, K. Li, M. Z. Qayyum, D. Yernool, W. Jiang, K. S. Murakami, Cryo-EM structure of Escherichia coli σ70 RNA polymerase and promoter DNA complex revealed a role of σ non-conserved region during the open complex formation. *Journal of Biological Chemistry*. **293**, 7367–7375 (2018).
25. J. Chen, S. Gopalkrishnan, C. Chiu, A. Y. Chen, E. A. Campbell, R. L. Gourse, W. Ross, S. A. Darst, E. coli TraR allosterically regulates transcription initiation by altering RNA polymerase conformation. *eLife*. **8** (2019), doi:10.7554/eLife.49375.

26. F. Wang, J. Shi, D. He, B. Tong, C. Zhang, A. Wen, Y. Zhang, Y. Feng, W. Lin, Structural basis for transcription inhibition by E. coli SspA. *Nucleic Acids Research*. **48**, 9931–9942 (2020).
27. B. A. Travis, K. M. Ramsey, S. M. Prezioso, T. Tallo, J. M. Wandzilak, A. Hsu, M. Borgnia, A. Bartesaghi, S. L. Dove, R. G. Brennan, M. A. Schumacher, Structural Basis for Virulence Activation of Francisella tularensis. *Molecular Cell*. **81**, 139-152.e10 (2021).
28. J. Shi, A. Wen, S. Jin, B. Gao, Y. Huang, Y. Feng, Transcription activation by a sliding clamp. *Nature Communications*. **12**, 1131–1131 (2021).
29. S. R. M., C. James, C. C. E., M. Brandon, S. Johanna, E. Mark, Y. L. Y., E. E. T., D. S. A., Structural origins of Escherichia coli RNA polymerase open promoter complex stability. *Proceedings of the National Academy of Sciences*. **118**, e2112877118–e2112877118 (2021).
30. F. Wang, Y. Feng, Z. Shang, W. Lin, A unique binding between SspA and RNAP β'NTH across low-GC Gram-negative bacteria facilitates SspA-mediated transcription regulation. *Biochemical and Biophysical Research Communications*. **583**, 86–92 (2021).
31. L. J. Lambert, Y. Wei, V. Schirf, B. Demeler, M. H. Werner, T4 AsiA blocks DNA recognition by remodeling σ70 region 4. *The EMBO Journal*. **23**, 2952–2962 (2004).
32. G. A. Patikoglou, L. F. Westblade, E. A. Campbell, V. Lamour, W. J. Lane, S. A. Darst, Crystal Structure of the Escherichia coli Regulator of σ70, Rsd, in Complex with σ70 Domain 4. *Journal of Molecular Biology*. **372**, 649–659 (2007).
33. A. G. Blanco, A. Canals, J. Bernués, M. Solà, M. Coll, The structure of a transcription activation subcomplex reveals how σ70 is recruited to PhoB promoters. *The EMBO Journal*. **30**, 3776–3785 (2011).
34. A. Malhotra, E. Severinova, S. A. Darst, Crystal Structure of a σ70 Subunit Fragment from E. coli RNA Polymerase. *Cell*. **87**, 127–136 (1996).
35. E. A. Campbell, O. Muzzin, M. Chlenov, J. L. Sun, C. A. Olson, O. Weinman, M. L. Trester-Zedlitz, S. A. Darst, Structure of the Bacterial RNA Polymerase Promoter Specificity σ Subunit. *Molecular Cell*. **9**, 527–539 (2002).
36. W. Li, C. E. M. Stevenson, N. Burton, P. Jakimowicz, M. S. B. Paget, M. J. Buttner, D. M. Lawson, C. Kleanthous, Identification and Structure of the Anti-sigma Factor-binding Domain of the Disulphide-stress Regulated Sigma Factor σR from Streptomyces coelicolor. *Journal of Molecular Biology*. **323**, 225–236 (2002).
37. A. J. Dombroski, W. A. Walter, M. T. J. Record, D. A. Siegele, C. A. Gross, Polypeptides containing highly conserved regions of transcription initiation factor sigma 70 exhibit specificity of binding to promoter DNA. *Cell*. **70**, 501–512 (1992).
38. A. J. Dombroski, W. A. Walter, C. A. Gross, Amino-terminal amino acids modulate sigma-factor DNA-binding activity. *Genes & development*. **7**, 2446–2455 (1993).
39. E. C. Schwartz, A. Shekhtman, K. Dutta, M. R. Pratt, D. Cowburn, S. Darst, T. W. Muir, A Full-Length Group 1 Bacterial Sigma Factor Adopts a Compact Structure Incompatible with DNA Binding. *Chemistry & Biology*. **15**, 1091–1103 (2008).
40. K. R. Vishwakarma, A.-M. Cao, Z. Morichaud, A. S. Perumal, E. Margeat, K. Brodolin, Single-molecule analysis reveals the mechanism of transcription activation in M. tuberculosis. *Science Advances*. **4**, eaao5498–eaao5498 (2018).
41. S. Callaci, T. Heyduk, Conformation and DNA Binding Properties of a Single-Stranded DNA Binding Region of σ70 Subunit from Escherichia coli RNA Polymerase Are Modulated by an Interaction with the Core Enzyme. *Biochemistry*. **37**, 3312–3320 (1998).
42. S. Callaci, E. Heyduk, T. Heyduk, Core RNA Polymerase from E. coli Induces a Major Change in the Domain Arrangement of the σ70 Subunit. *Molecular Cell*. **3**, 229–238 (1999).
43. T. M. Gruber, D. Markov, M. M. Sharp, B. A. Young, C. Z. Lu, H. J. Zhong, I. Artsimovitch, K. M. Geszvain, T. M. Arthur, R. R. Burgess, R. Landick, K. Severinov, C. A. Gross, Binding of the Initiation Factor σ70 to Core RNA Polymerase Is a Multistep Process. *Molecular Cell*. **8**, 21–31 (2001).
44. K. Konstantin, M. Leonid, N.-M. Anita, D. S. L., R. Dragana, N. B. E., H. Ann, H. Tomasz, S. Konstantin, A Role for Interaction of the RNA Polymerase Flap Domain with the σ Subunit in Promoter Recognition. *Science*. **295**, 855–857 (2002).
45. A. Feklistov, N. Barinova, A. Sevostyanova, E. Heyduk, I. Bass, I. Vvedenskaya, K. Kuznedelov, E. Merkienė, E. Stavrovskaya, S. Klimašauskas, V. Nikiforov, T. Heyduk, K. Severinov, A. Kulbachinskiy, A Basal Promoter Element Recognized by Free RNA Polymerase σ Subunit Determines Promoter Recognition by RNA Polymerase Holoenzyme. *Molecular Cell*. **23**, 97–107 (2006).
46. M. K. S., M. Shoko, C. E. A., M. Oriana, D. S. A., Structural Basis of Transcription Initiation: An RNA Polymerase Holoenzyme-DNA Complex. *Science*. **296**, 1285–1290 (2002).

47. D. G. Vassylyev, S. Sekine, O. Laptenko, J. Lee, M. N. Vassylyeva, S. Borukhov, S. Yokoyama, Crystal structure of a bacterial RNA polymerase holoenzyme at 2.6 Å resolution. *Nature*. **417**, 712–719 (2002).
48. M. K. S., M. Shoko, D. S. A., Structural Basis of Transcription Initiation: RNA Polymerase Holoenzyme at 4 Å Resolution. *Science*. **296**, 1280–1284 (2002).
49. T. Ha, T. Enderle, D. F. Ogletree, D. S. Chemla, P. R. Selvin, S. Weiss, Probing the Interaction between Two Single Molecules: Fluorescence Resonance Energy Transfer between a Single Donor and a Single Acceptor. *Proceedings of the National Academy of Sciences*. **93**, 6264–6268 (1996).
50. E. Lerner, T. Cordes, A. Ingargiola, Y. Alhadid, S. Chung, X. Michalet, S. Weiss, Toward dynamic structural biology: Two decades of single-molecule Förster resonance energy transfer. *Science*. **359**, eaan1133–eaan1133 (2018).
51. N. Kalisman, C. M. Adams, M. Levitt, Subunit order of eukaryotic TRiC/CCT chaperonin by cross-linking, mass spectrometry, and combinatorial homology modeling. *Proceedings of the National Academy of Sciences*. **109**, 2884–2889 (2012).
52. K. Murakami, H. Elmlund, N. Kalisman, D. A. Bushnell, C. M. Adams, M. Azubel, D. Elmlund, Y. Levi-Kalisman, X. Liu, B. J. Gibbons, M. Levitt, R. D. Kornberg, Architecture of an RNA polymerase II transcription pre-initiation complex. *Science*. **342** (2013), doi:10.1126/science.1238724.
53. A. Leitner, L. A. Joachimiak, P. Unverdorben, T. Walzthoeni, J. Frydman, F. Förster, R. Aebersold, *Proceedings of the National Academy of Sciences*, in press, doi:10.1073/pnas.1320298111.
54. R. G. Walker, X. Deng, J. T. Melchior, J. Morris, P. Tso, M. K. Jones, J. P. Segrest, T. B. Thompson, W. S. Davidson, The Structure of Human Apolipoprotein A-IV as Revealed by Stable Isotope-assisted Cross-linking, Molecular Dynamics, and Small Angle X-ray Scattering. *Journal of Biological Chemistry*. **289**, 5596–5608 (2014).
55. Z. Liu, Z. Gong, Y. Cao, Y. H. Ding, M. Q. Dong, Y. B. Lu, W. P. Zhang, C. Tang, Characterizing Protein Dynamics with Integrative Use of Bulk and Single-Molecule Techniques. *Biochemistry*. **57**, 305–313 (2018).
56. D. B. Lima, J. T. Melchior, J. Morris, V. C. Barbosa, J. Chamot-Rooke, M. Fioramonte, T. A. C. B. Souza, J. S. G. Fischer, F. C. Gozzo, P. C. Carvalho, W. S. Davidson, Characterization of homodimer interfaces with cross-linking mass spectrometry and isotopically labeled proteins. *Nature Protocols*. **13**, 431–458 (2018).
57. M. Slavin, N. Kalisman, "Structural analysis of protein complexes by cross-linking and mass spectrometry" in *Methods in Molecular Biology*, J. A. Marsh, Ed. (Springer New York, New York, 2018), vol. 1764, pp. 173–183.
58. D. Duhovny, R. Nussinov, H. J. Wolfson, "Efficient Unbound Docking of Rigid Molecules BT - Algorithms in Bioinformatics" in, R. Guigó, D. Gusfield, Eds. (Springer Berlin Heidelberg, Berlin, Heidelberg, 2002), pp. 185–200.
59. D. Schneidman-Duhovny, Y. Inbar, R. Nussinov, H. J. Wolfson, PatchDock and SymmDock: servers for rigid and symmetric docking. *Nucleic Acids Research*. **33**, W363–W367 (2005).
60. P. D. Harris, A. Narducci, C. Gebhardt, T. Cordes, S. Weiss, E. Lerner, Multi-parameter photon-by-photon hidden Markov modeling. *Nature Communications*. **13**, 1000–1000 (2022).
61. J. Mukhopadhyay, A. N. Kapanidis, V. Mekler, E. Kortkhonjia, Y. W. Ebright, R. H. Ebright, Translocation of σ70 with RNA Polymerase during Transcription: Fluorescence Resonance Energy Transfer Assay for Movement Relative to DNA. *Cell*. **106**, 453–463 (2001).
62. S. Kim, A. M. Streets, R. R. Lin, S. R. Quake, S. Weiss, D. S. Majumdar, High-throughput single-molecule optofluidic analysis. *Nature Methods*. **8**, 242–242 (2011).
63. M. Baek, F. DiMaio, I. Anishchenko, J. Dauparas, S. Ovchinnikov, G. R. Lee, J. Wang, Q. Cong, L. N. Kinch, R. D. Schaeffer, C. Millán, H. Park, C. Adams, C. R. Glassman, A. DeGiovanni, J. H. Pereira, A. V. Rodrigues, A. A. van Dijk, A. C. Ebrecht, D. J. Opperman, T. Sagmeister, C. Buhlheller, T. Pavkov-Keller, M. K. Rathinaswamy, U. Dalwadi, C. K. Yip, J. E. Burke, K. C. Garcia, N. V. Grishin, P. D. Adams, R. J. Read, D. Baker, Accurate prediction of protein structures and interactions using a three-track neural network. *Science*. **373**, 871–876 (2021).
64. J. Jumper, R. Evans, A. Pritzel, T. Green, M. Figurnov, O. Ronneberger, K. Tunyasuvunakool, R. Bates, A. Žídek, A. Potapenko, A. Bridgland, C. Meyer, S. A. A. Kohl, A. J. Ballard, A. Cowie, B. Romera-Paredes, S. Nikolov, R. Jain, J. Adler, T. Back, S. Petersen, D. Reiman, E. Clancy, M. Zielinski, M. Steinegger, M. Pacholska, T. Berghammer, S. Bodenstein, D. Silver, O. Vinyals, A. W. Senior, K. Kavukcuoglu, P. Kohli, D. Hassabis, Highly accurate protein structure prediction with AlphaFold. *Nature*. **596**, 583–589 (2021).
65. M. Varadi, S. Anyango, M. Deshpande, S. Nair, C. Natassia, G. Yordanova, D. Yuan, O. Stroe, G. Wood, A. Laydon, A. Žídek, T. Green, K. Tunyasuvunakool, S. Petersen, J. Jumper, E. Clancy, R. Green, A. Vora, M. Lutfi, M. Figurnov, A. Cowie, N. Hobbs, P. Kohli, G. Kleywegt, E. Birney, D. Hassabis, S. Velankar, AlphaFold

Protein Structure Database: massively expanding the structural coverage of protein-sequence space with high-accuracy models. *Nucleic Acids Research*. **50**, D439–D444 (2022).
66. R. Wu, F. Ding, R. Wang, R. Shen, X. Zhang, S. Luo, C. Su, Z. Wu, Q. Xie, B. Berger, J. Ma, J. Peng, *bioRxiv*, in press, doi:10.1101/2022.07.21.500999.
67. N. Opalka, J. Brown, W. J. Lane, K.-A. F. Twist, R. Landick, F. J. Asturias, S. A. Darst, Complete Structural Model of Escherichia coli RNA Polymerase from a Hybrid Approach. *PLOS Biology*. **8**, e1000483–e1000483 (2010).
68. E. Jurrus, D. Engel, K. Star, K. Monson, J. Brandi, L. E. Felberg, D. H. Brookes, L. Wilson, J. Chen, K. Liles, M. Chun, P. Li, D. W. Gohara, T. Dolinsky, R. Konecny, D. R. Koes, J. E. Nielsen, T. Head-Gordon, W. Geng, R. Krasny, G.-W. Wei, M. J. Holst, J. A. McCammon, N. A. Baker, Improvements to the APBS biomolecular solvation software suite. *Protein Science*. **27**, 112–128 (2018).
69. E. Krissinel, K. Henrick, Inference of Macromolecular Assemblies from Crystalline State. *Journal of Molecular Biology*. **372**, 774–797 (2007).
70. P. Landini, T. Egli, J. Wolf, S. Lacour, sigmaS, a major player in the response to environmental stresses in Escherichia coli: role, regulation and mechanisms of promoter recognition. *Environmental Microbiology Reports*. **6**, 1–13 (2014).
71. K. Joron, J. Zamel, S. Dvir, N. Kalisman, E. Lerner, The structural basis for the self-inhibition of DNA binding by apo-σ70 - smFRET raw data and analyses pipeline (2022), (available at https://doi.org/10.5281/zenodo.7173886).

Acknowledgments

The plasmid of the Cys-less σ^{70}, from which we prepared the doubly-labeled σ^{70} variant for our smFRET measurements, was provided to us as a gift from the laboratory of Dr. Shimon Weiss, UCLA. We would like to thank the following: (i) Dr. Dina Schneidman and Merav Braitbard for providing PatchDock and assisting in the docking procedures, (ii) Dr. Paul David Harris for consultation regarding mpH^{2}MM analyses of smFRET data, (iii) Dr. Emmanuel Margeat for discussions regarding past smFRET measurements of apo-σ^{70} and for providing us the raw data of these previous measurements for comparison against our newly acquired data, and (iv) Dr. Shimon Weiss for fruitful discussions and for inspecting the text of this work.

Funding

The Israel Science Foundation grant 1768/15 (N.K.)

The National Institute of Health grant R01 GM130942 (E.L. as a subaward)

Yad Hanadiv scholarship (K.J.)

Author contributions

Analytical tools: NK

Protein purification: KJ, SD

Experimental data: KJ, JZ, SD

Analysis of experimental data: KJ, EL

Writing – original draft: EL, KJ

Writing – reviewing & editing: NK, JZ, SD

Competing interests: All authors declare no competing interests.

Data and materials availability: SmFRET data and analysis pipeline in Jupyter notebooks stored in Zenodo – https://doi.org/10.5281/zenodo.7173886(*71*). CLMS data – available at Proteomics Identification Database (PRIDE), titled "the structural basis for the self-inhibition of DNA binding by apo-σ70 - CLMS data" - https://www.ebi.ac.uk/pride/archive/projects/PXD037183. Model structures – available at PDB-Dev as accession codes PDBDEV_00000125 and PDBDEV_00000126 – https://pdb-dev.wwpdb.org/entry.html?PDBDEV_00000125 and https://pdb-dev.wwpdb.org/entry.html?PDBDEV_00000126.

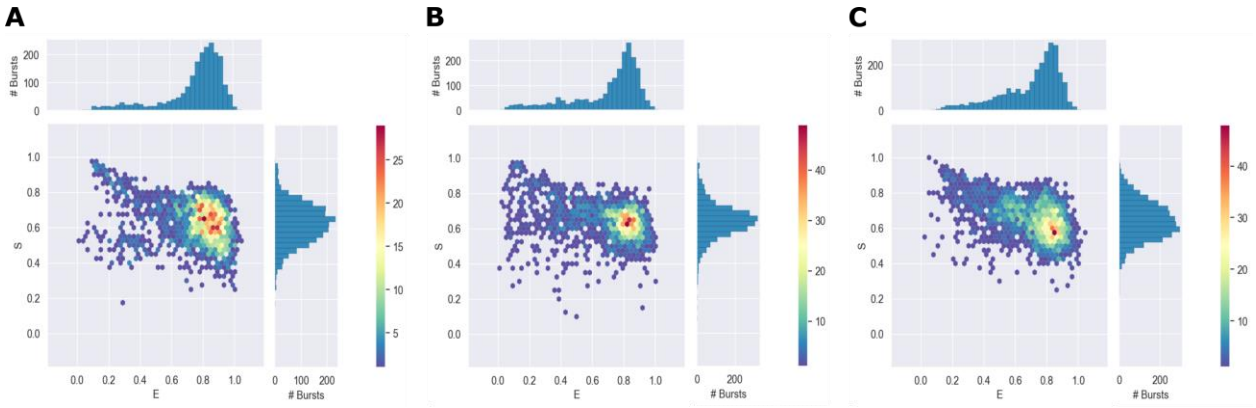

Fig. 1. Apo-σ^{70} is unable to specifically bind dsDNA. Single molecule concentration of apo-σ^{70} labeled at residues 442C and 579C with ATTO 550 and ATTO 643. (**A**) Apo-σ^{70}, a major population exist at high FRET with a tale towards lower FRET efficiencies. (**B**) Apo-σ^{70} with 100 nM dsDNA, exhibits no significant change in the major high FRET population. (**C**) Apo-σ^{70} with 2 μM dsDNA, exhibits a slight increase in sub-population with lower FRET.

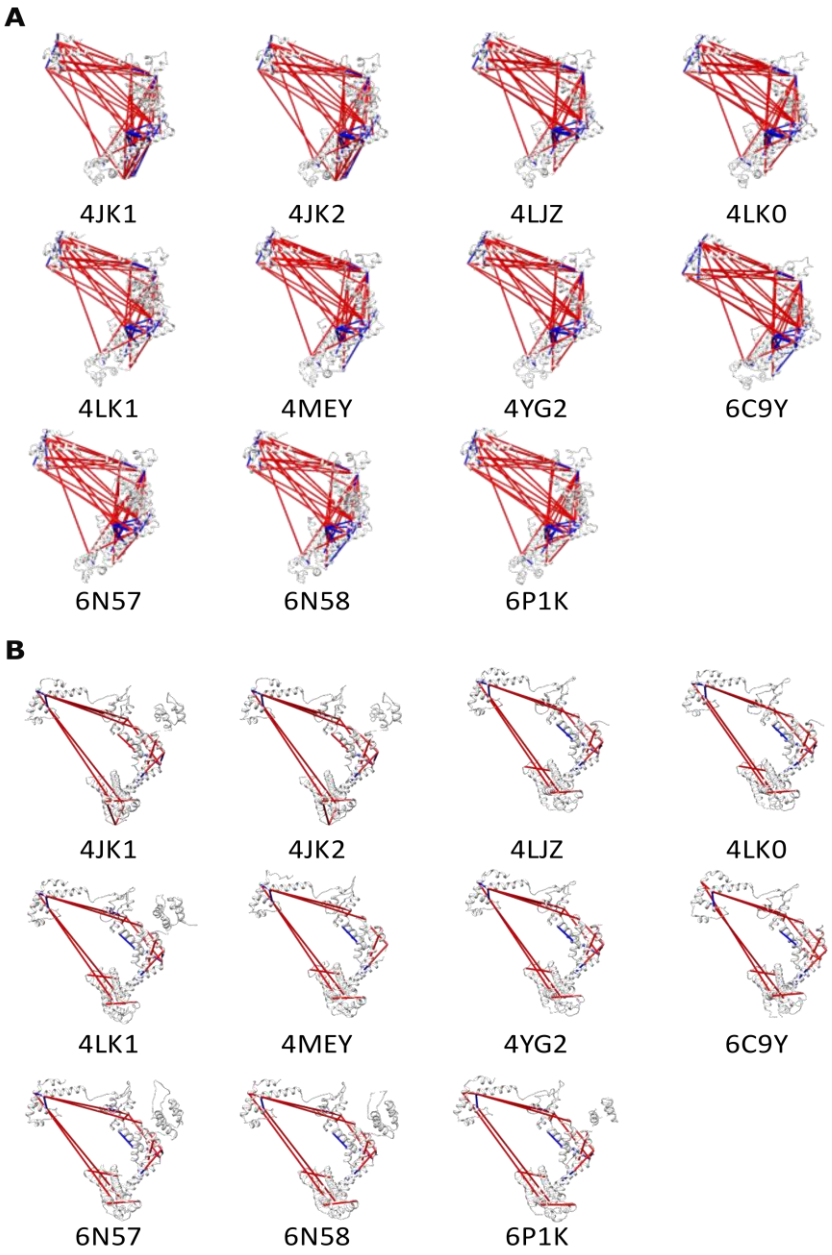

Fig. 2. *In vitro* apo-σ^{70} crosslinked pairs of residues displayed on top of σ^{70} PDB structures within the RNAP holoenzyme. (**A**) BS^3 crosslinked pairs and (**B**) DMTMM crosslinked pairs. Blue and red – distances between pairs of crosslinked residues that are within or are not within the C_α-C_α distance which is covered by the crosslinker, respectivly.

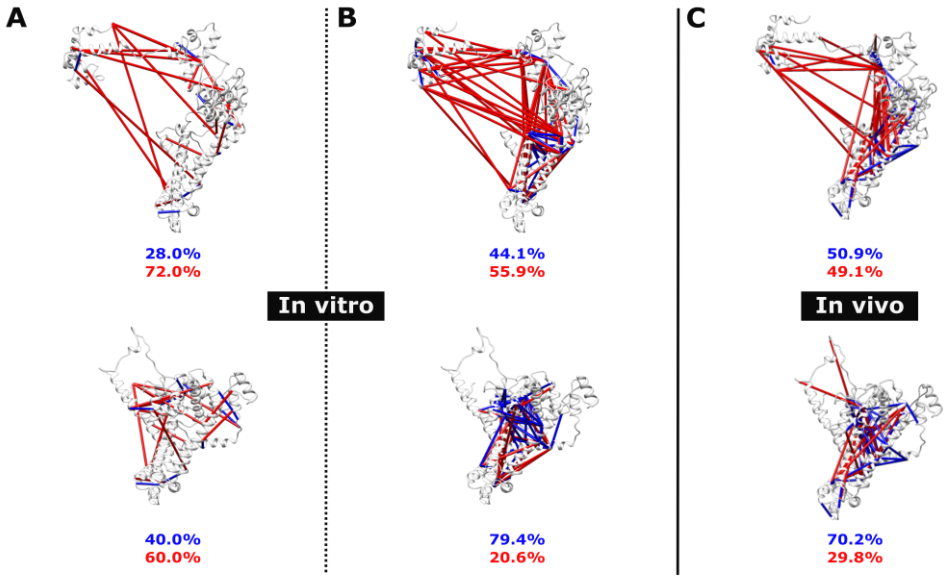

Fig. 3. Apo-σ^{70} *in vitro* and *in vivo* CL-MS data have a higher satistfction rate with the compact structure. RossetaFold model (top row), and compact PatchDock structure 1 (bottom row). (**A**) *In vitro* BS^3 and (**B**) DMTMM crosslinked pairs of residues. (**C**) *In vivo* DSS crosslinked pairs of residues. Blue and red – distances between pairs of crosslinked residues that are within or are not within the C_α-C_α distance which is covered by the crosslinker, respectivly.

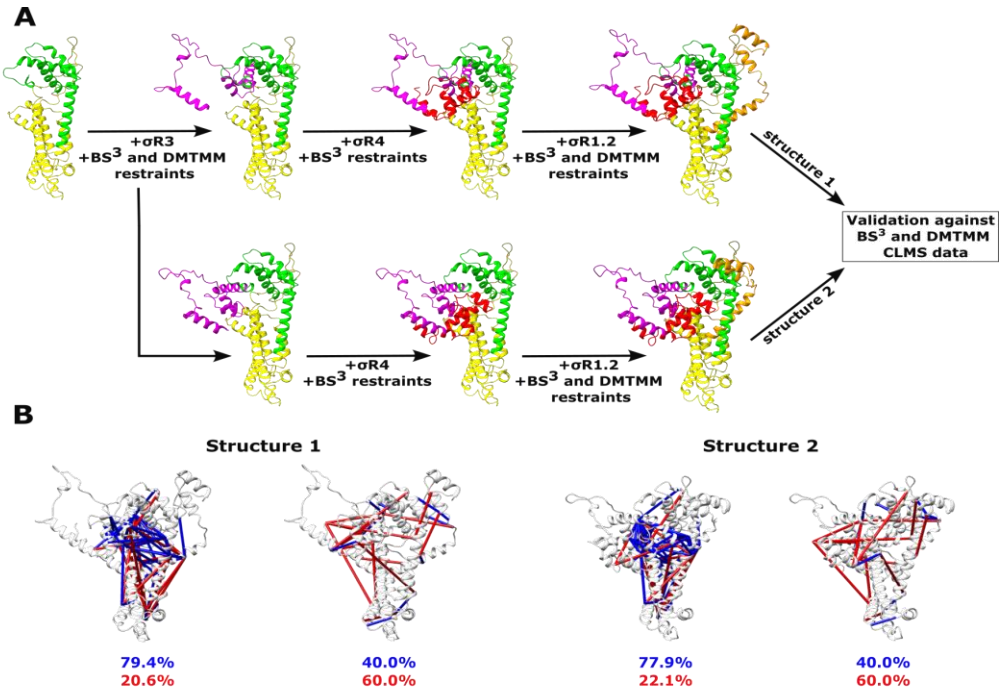

Fig. 4. Stepwise results of Patch-Docking σ^{70} regions using the CL-MS spatial information as restraints. (**A**) σNER in yellow, σR2 in green, σR3 in magenta, σR4 in red and σR1.2 in orange. In each step a σ^{70} region is introduced to the previous result, together with CL-MS derived restraints. (**B**) The two structures retrieved from PatchDock. For each structure, the BS^3 crosslinking data is displayed on the left, while DMTMM data is on the right. Blue and red – distances between pairs of crosslinked residues that are within or are not within the C_α-C_α distance which is covered by the crosslinker, respectivly.

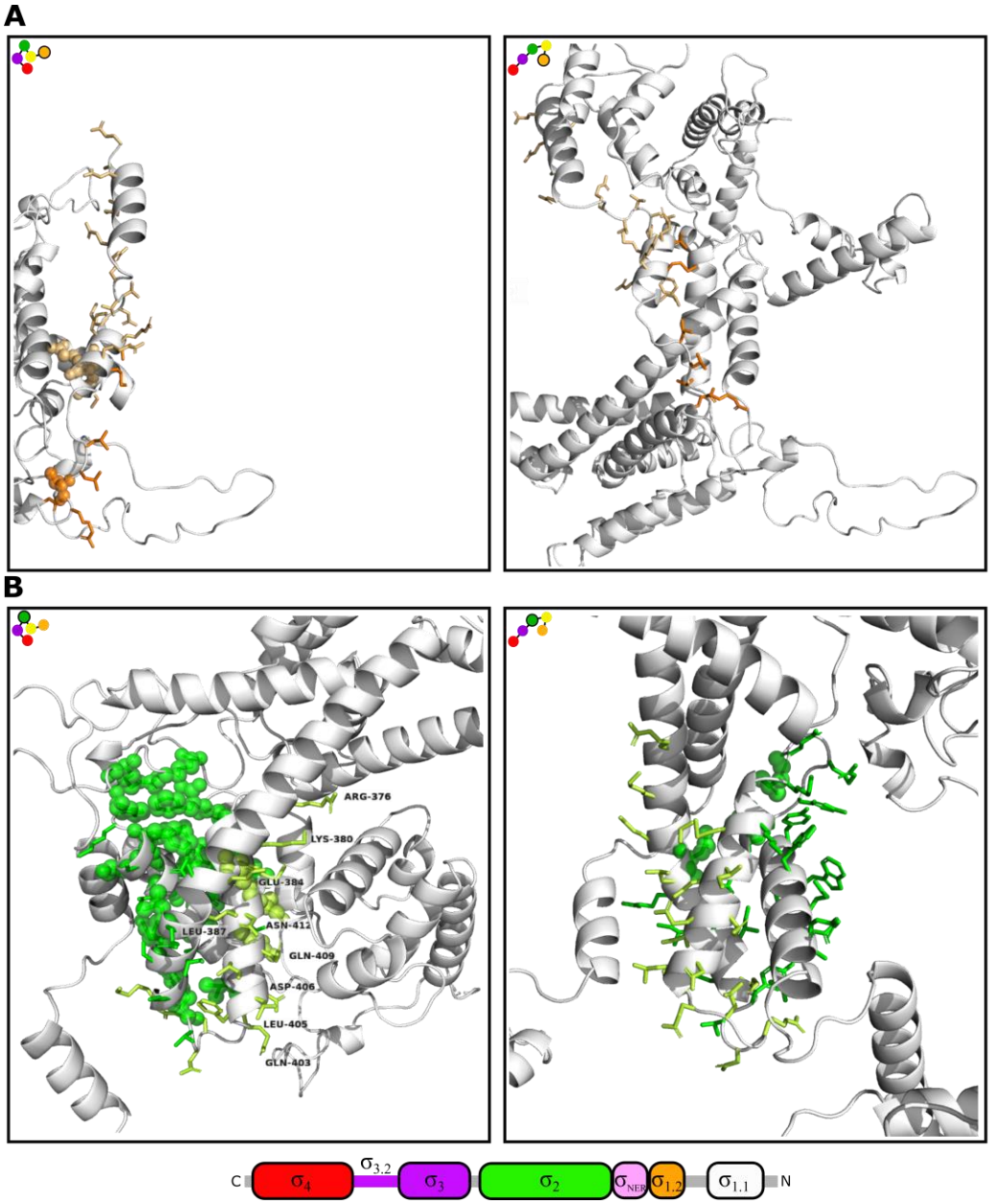

Fig. 5. σR1.2 and σR2 residues that interact with RNAP and DNA in the RNAP-bound state. Solvent exposed residues are displayed as sticks, while residues buried inside the structure are displayed as spheres. Left panels – compact apo-σ^{70}, right panels – extended RNAP-bound σ^{70}. Illustrations of the two forms are provided by connected dots, with colors that match the σ^{70}'s specific region color presented at the bottom. (**A**) Residues that potentially interact with the RNAP subunit β` or with the discriminator element are shown in bright and dark orange, respectivly. (**B**) Residues interacting with the β and β` subunits or the -10 promoter element are shown in bright and dark green, respectivly (labeled residues are exposed to solvent – R376, K380, E384, L387, Q403, L405, D406, Q409 and N412).

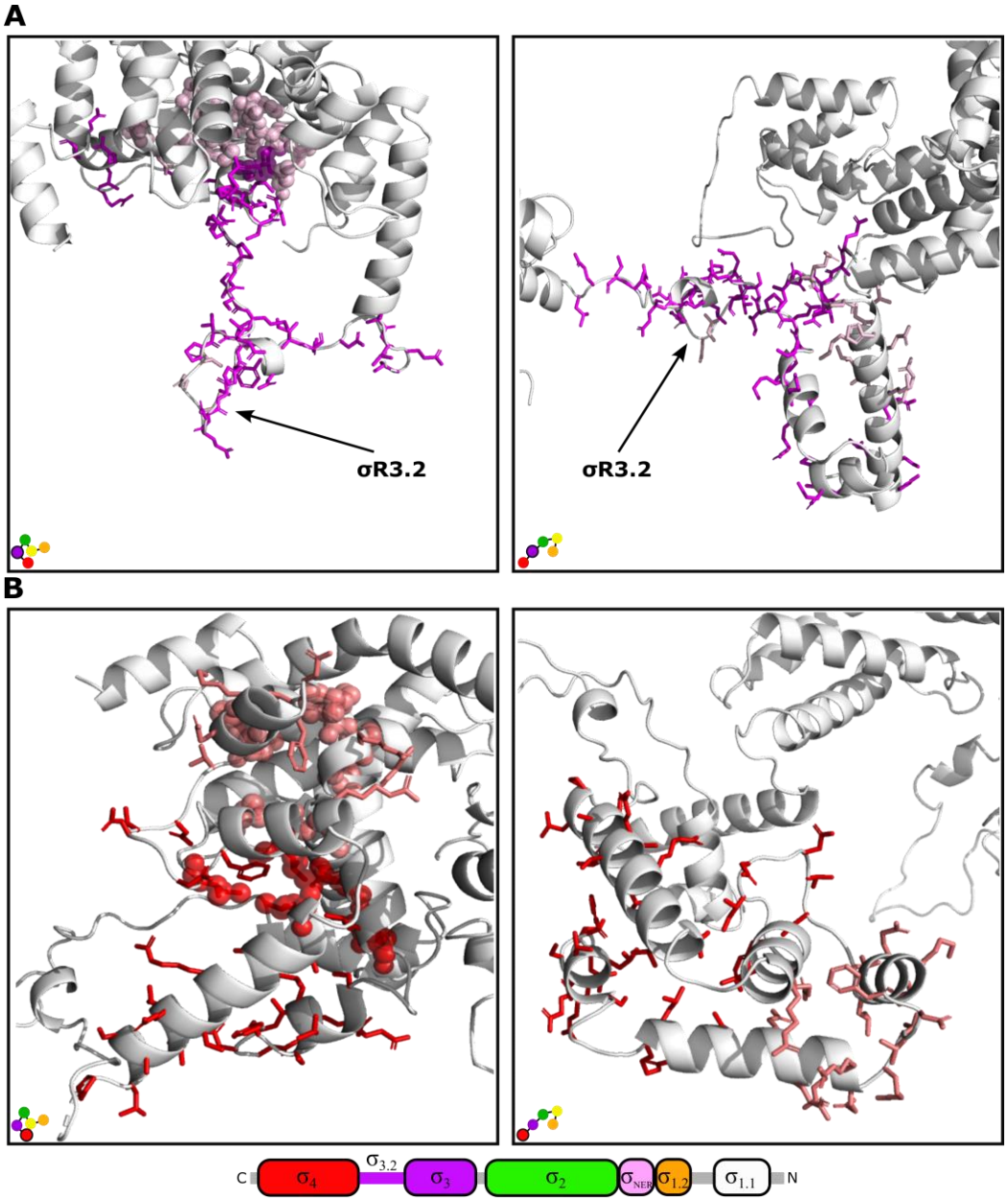

Fig. 6. σR3 and σR4 residues that interact with RNAP and DNA in the RNAP-bound state. Solvent-exposed residues on the exterior surface of σ^{70} are displayed as sticks and residues buried inside the structure are displayed as spheres. Left panels – compact apo-σ^{70}, right panels – extended RNAP-bound σ^{70}. Illustrations of the two forms are provided by connected dots, with colors that match the σ^{70}'s specific region color presented at the bottom. (**A**) Residues that potentially interact with the β and β` subunits or with the -10 extended element are shown in magenta or pink, respectivly. (**B**) Residues interacting with the β and β` subunits or with the -35 promoter element are shown in dark or light red, respectivly.